Spin Fluctuations Drive the Inverse Magnetocaloric Effect in Mn_5Si_3

N. Biniskos,[1,2,*] K. Schmalzl,[1] S. Raymond,[2,†] S. Petit,[3] P. Steffens,[4] J. Persson,[5] and T. Brückel[5,6]

[1]*Forschungszentrum Jülich GmbH, Jülich Centre for Neutron Science at ILL, 71 avenue des Martyrs, 38000 Grenoble, France*

[2]*Université Grenoble Alpes, CEA, INAC, MEM, 38000 Grenoble, France*

[3]*Laboratoire Léon Brillouin, CEA, CNRS, Université Paris–Saclay, CE–Saclay, F-91191 Gif sur Yvette, France*

[4]*Institut Laue-Langevin, 71 avenue des Martyrs, 38000 Grenoble, France*

[5]*Forschungszentrum Jülich GmbH, Jülich Centre for Neutron Science (JCNS-2) and Peter Grünberg Institut (PGI-4), JARA-FIT, 52425 Jülich, Germany*

[6]*Forschungszentrum Jülich GmbH, Jülich Centre for Neutron Science at MLZ, Lichtenbergstrasse 1, 85748 Garching, Germany*

(Received 30 January 2018; published 22 June 2018)

Inelastic neutron scattering measurements are performed on single crystals of the antiferromagnetic compound Mn_5Si_3 in order to investigate the relation between the spin dynamics and the magneto-thermodynamics properties. It is shown that, among the two stable antiferromagnetic phases of this compound, the high temperature one has an unusual magnetic excitation spectrum where propagative spin waves and diffuse spin fluctuations coexist. Moreover, it is evidenced that the inverse magnetocaloric effect of Mn_5Si_3, the cooling by adiabatic magnetization, is associated with field induced spin fluctuations.

DOI: 10.1103/PhysRevLett.120.257205

Caloric effects are inherent to magnetization processes. The degree of order of a magnetic system determines the number of accessible states, which in turn defines its magnetic entropy. The Maxwell relation $(\partial S/\partial H)_{T,p} = (\partial M/\partial T)_{H,p}$ relates the entropy $S(H,T)$ to the magnetization $M(H,T)$ of a system under constant pressure [1]. This shows that any temperature dependence of the magnetization is coupled to an entropy change when varying the magnetic field. Two well-known realizations are the adiabatic demagnetization of paramagnetic (PM) salts to reach subkelvin temperatures [2] and the giant magnetocaloric effect (MCE) observed near room temperature magnetostructural phase transitions [3–5]. The latter effect can be potentially used for magnetic refrigeration applications in daily life [6].

Alternatively, in some compounds cooling can be achieved by adiabatic magnetization, a less common effect, the inverse MCE. The discovery of a large inverse MCE around room temperature has attracted interest since it provides added flexibility in the material and functional device design [7,8]. Systems of interest undergo a first-order magnetic transformation between distinct magnetic phases: antiferromagnetic (AFM) to ferrimagnetic transitions [9,10], AFM to FM transitions [11–13], and collinear to noncollinear AFM transitions like in Mn_5Si_3 [14], the subject of this Letter.

This Letter provides new insight into the origin of the inverse MCE in Mn_5Si_3 by relating it to the spin dynamics observed by inelastic neutron scattering (INS) from single crystals. Our experiments revealed that the low temperature noncollinear AFM1 phase is characterized by well-defined spin waves, while the higher temperature collinear AFM2 phase is characterized by a coexistence of spin waves and diffuse spin fluctuations. Furthermore, the application of a magnetic field in the AFM1 phase induces spin fluctuations by restoring the AFM2 phase. The entropy release associated with these spin fluctuations points to their importance in the inverse MCE in Mn_5Si_3.

In its high temperature PM state, Mn_5Si_3 crystallizes in the hexagonal space group $P6_3/mcm$ with two distinct crystallographic positions for Mn atoms (sites Mn1 and Mn2) [15]. Two first-order phase transitions towards antiferromagnetic phases occur at $T_{N_2} \approx 100$ K (AFM2) and $T_{N_1} \approx 66$ K (AFM1), respectively [14]. Associated with the AFM2 ordering, a change of crystal structure to the orthorhombic space group $Ccmm$ occurs and Mn2 divides into two sets of inequivalent positions. Magnetic reflections in this cell follow the condition $h + k$ odd corresponding to the magnetic propagation vector $\mathbf{k} = (0, 1, 0)$ [16]. In this phase, the Mn1 atoms and one third of the Mn2 atoms have no ordered moments, and the remaining Mn2 atoms have their magnetic moments aligned almost parallel and antiparallel to the b axis [16] [see Fig. 1(a)]. In what follows, AFM2 is named the collinear phase. Another structural distortion occurs concomitantly with the AFM1 ordering towards an orthorhombic cell without inversion symmetry (space group $Cc2m$) [17]. The magnetic moments reorient in a highly noncollinear and noncoplanar arrangement, while the propagation vector remains the same. Mn1 atoms acquire a magnetic moment, and one third of the Mn2 atoms still have no ordered moments, just as in the AFM2 phase [see Fig. 1(a)]. The remaining Mn2 atoms carry a different moment, depending on their site. Neutron diffraction [15,18] and macroscopic measurements [19,20] indicate that Mn_5Si_3 undergoes several magnetic phase transitions under magnetic field and temperature. The

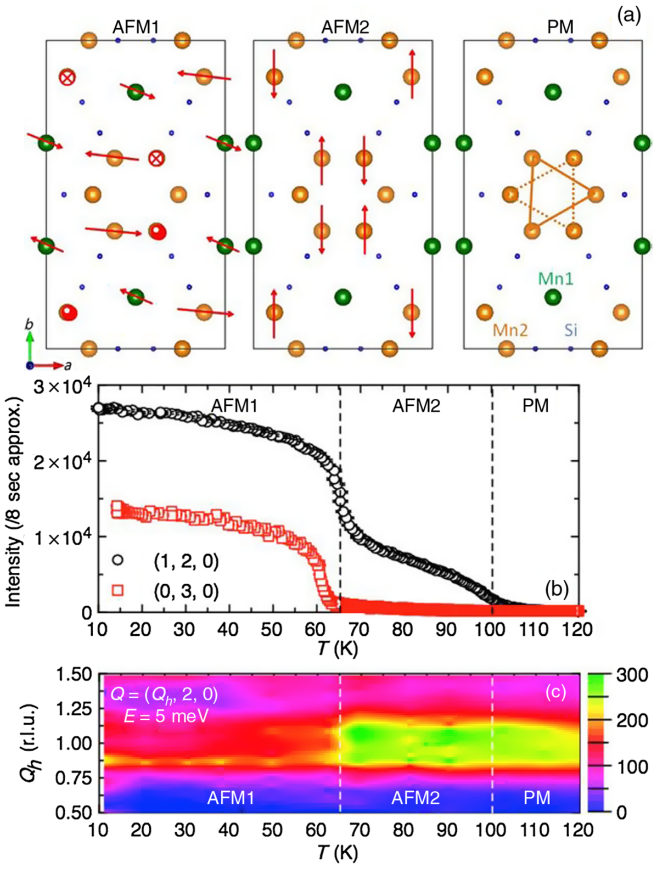

FIG. 1. (a) Projection of the structure of Mn_5Si_3 in the (a, b) plane of the orthorhombic cell according to single crystal neutron diffraction data [16,17]. The triangles with continuous and dashed lines are located in different planes separated by $c/2$. The red symbols ⊗ and ⊙ in the AFM1 phase indicate magnetic moments pointing in and out of the page, respectively. (b) Temperature dependence of the purely magnetic (1, 2, 0) and (0, 3, 0) Bragg peak intensities. (c) Color-coded intensity plot of the INS data collected at a constant energy transfer of 5 meV as a function of $\mathbf{Q} = (Q_h, 2, 0)$ and temperature. Data were collected with an unpolarized neutron beam using the three-axis spectrometer 2T1. In the inelastic spectra, the background is subtracted and the measured intensity is corrected by the detailed balance factor.

inverse MCE is associated with the AFM1-AFM2 phase transition and the magnetic entropy change is $\approx 3\ \mathrm{J\,K^{-1}\,kg^{-1}}$ for a field change from 0 to 5 T [14]. Additional interest in Mn_5Si_3 lies in its electronic transport properties, where the noncollinear AFM1 phase is responsible for the anomalous Hall effect [20–22].

INS measurements were performed on single crystal samples; for experimental details, see the Supplemental Material [23]. The temperature dependence of the purely magnetic (1, 2, 0) and (0, 3, 0) Bragg peak intensities are shown in Fig. 1(b). (1, 2, 0) marks the onset of AFM2 ordering. Neutron scattering is sensitive to magnetic moments or fluctuations perpendicular to the scattering vector. The $\mathbf{Q}$ vector of (0, 3, 0) is almost parallel to the magnetic moments in the AFM2 phase, and the associated Bragg peak intensity therefore nearly vanishes. However, this $\mathbf{Q}$ position is convenient to detect the AFM1 transition. A color-coded intensity map of the INS intensity measured for a constant energy transfer of $E = 5$ meV as a function of $\mathbf{Q} = (Q_h, 2, 0)$ and T is shown in Fig. 1(c). The PM scattering consists of a broad peak centered at the magnetic center $Q_h = 1$ r.l.u., the signature of a correlated diffuse signal. Short-range spin correlations persist in the PM state, giving rise to the observed inelastic response. The shape of the scattering of the AFM2 phase resembles that of the PM state, as no marked change in the dynamical response occurs at T_{N_2}. By contrast, AFM1 ordering is characterized by a strong modification of the spectrum leading to sharp spin-wave peaks identified through the ridges at $Q_h = 0.87$ r.l.u. and $Q_h = 1.13$ r.l.u., with the former being more prominent due to the instrumental resolution focusing conditions. Hence, the spin excitation spectrum is markedly different in the two magnetically ordered phases. The same observations stem from the cuts obtained along the a direction at another energy transfer of $E = 3$ meV and shown in Fig. 2(d) for selected temperatures in the different

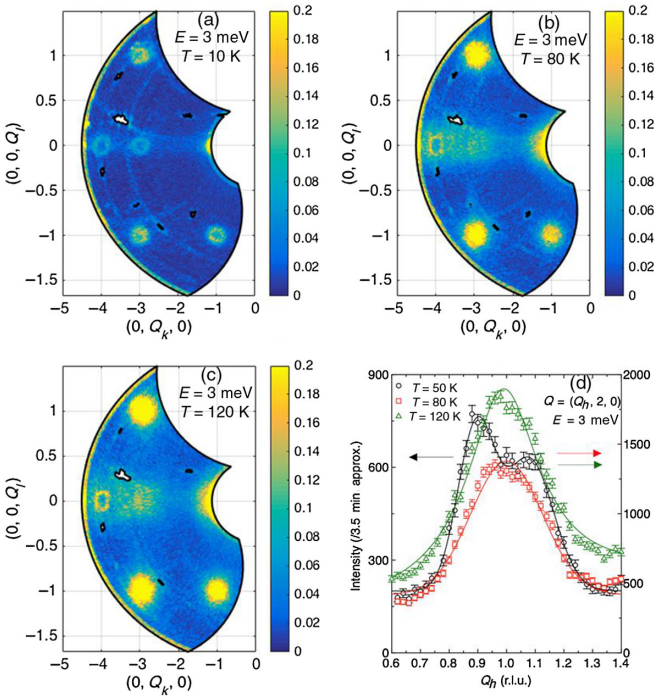

FIG. 2. (a)–(c) FlatCone measurements in the scattering plane (b, c) taken with the three-axis spectrometer ThALES in the AFM1 (10 K) and AFM2 (80 K) phases and in the PM (120 K) state at a constant energy transfer of 3 meV. The "holes" in the spectra correspond to spurious scattering that has been masked during the data evaluation. (d) Raw data obtained with the three-axis spectrometer IN12 with an unpolarized neutron beam around $\mathbf{Q} = (Q_h, 2, 0)$ at a constant energy transfer of 3 meV. Lines in the AFM1 phase (50 K) and in the PM state (120 K) indicate fits with Gaussian and Lorentzian functions, respectively. The line in the AFM2 phase (80 K) is a guide for the eyes.

phases (cuts along the b and c high symmetry directions are shown in the Supplemental Material [23]).

To confirm this observation, INS spectra were collected in large portions of the reciprocal space in the (b, c) scattering plane for $E = 3$ meV at three different temperatures corresponding to the PM state ($T = 120$ K), the collinear AFM2 phase ($T = 80$ K) and the noncollinear AFM1 phase ($T = 10$ K). In the AFM1 phase, the rings in Fig. 2(a) represent intense phonon and spin-wave scattering originating from the structural ($h + k$ even) and magnetic ($h + k$ odd) zone centers, respectively. Consistent with Fig. 1(c), the spin excitation spectrum differs in the AFM1 and AFM2 phases for the inelastic spectra that originate from the magnetic Bragg peaks that exist in the two phases [e.g., (0, 3, 1), (0, 1, 1)]. While in the AFM1 phase clear rings indicate spin-wave scattering [see Fig. 2(a)], the signal in the AFM2 phase [the bright yellow spots in Fig. 2(b)] resembles the one of the PM state [Fig. 2(c)]. Additional spectra at different energies are provided in the Supplemental Material [23] in order to demonstrate the dispersive nature of the spin waves in the AFM1 phase and the diffusive nature of the spin fluctuations in the PM state.

The spin dynamics of the AFM2 phase is very peculiar: it is, at first sight, constituted not of discrete modes but of a broad continuum of states. In order to get more insight concerning this behavior and to compare it with the seemingly identical PM spin dynamics, spectra were collected using polarized INS methods. In such an experiment, the polarization of the incident neutron beam is consecutively turned into different directions, which gives access to different neutron cross sections. The corresponding measurement channels are canonically labeled SF_{xx}, SF_{yy}, and SF_{zz}, where SF stands for spin flip (see the details in the Supplemental Material [23]).

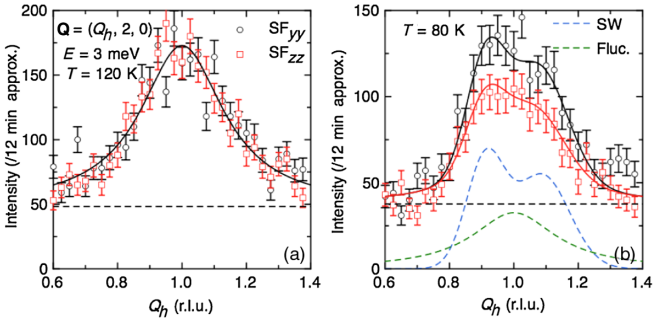

FIG. 3. Inelastic spectra at a constant energy transfer of 3 meV around $\mathbf{Q} = (Q_h, 2, 0)$ obtained with polarized neutrons in the PM state (120 K) and in the AFM2 phase (80 K) with IN12. (a) In the PM state (120 K), the solid line corresponds to a Lorentzian function fit. (b) In the AFM2 phase (80 K), the solid lines represent overall fits and the dashed lines the individual signal from spin waves (SW) and spin fluctuations (Fluc.) (see the details in the Supplemental Material [23]). The horizontal dashed line indicates the background level.

Figure 3 illustrates spectra collected around $\mathbf{Q} = (Q_h, 2, 0)$ at 80 K (AFM2) and 120 K (PM) for the SF_{yy} and SF_{zz} channels (SF_{xx} is shown for the AFM2 phase in the Supplemental Material [23]). The spectra in the PM state at 120 K are identical for the two polarization channels SF_{yy} and SF_{zz}, a result which indicates isotropic spin fluctuations. By contrast, the spectra in the AFM2 phase at 80 K are different for the two polarization channels concerning intensities and line shapes. This indicates that the magnetic excitation spectrum differs between the AFM2 phase and the PM state, a fact that was not evidenced by the unpolarized INS data shown above [see Fig. 2(d) and the Supplemental Material [23]]. Moreover, the better wave-vector resolution achieved with the setup used to collect the polarized INS data allows us to reveal the flat top shape of the peaks at 80 K. This hints at a signal composed of several ill-resolved peaks. Taken together, this information points to the fact that the signal in the AFM2 phase is composed of different components.

The simplest hypothesis to consider is that it is composed of spin waves coexisting with spin fluctuations. This natural assumption stems from the nature of the AFM2 magnetic phase with mixed magnetic and nonmagnetic sites. In order to examine this assumption on quantitative grounds, a simultaneous fit of the data obtained in the two channels SF_{yy} and SF_{zz} was performed. With such a fit, the dimensionality of the parameter space is decreased (see the equations in the Supplemental Material [23]). It is, furthermore, assumed that the spin fluctuations are isotropic at 80 K [as demonstrated at 120 K; see Fig. 3(a)] and that the spin-wave precession is isotropic around the b axis. The resulting fit shown in Fig. 3(b) for 80 K allows us to separate the proportion of spin waves (the blue dashed line) and spin fluctuations (the green dashed line) composing the overall signal. The data are well described by our model and, since the polarized INS cross sections convey stringent fitting conditions, the model gives credit to the hypothesis of the coexistence of spin waves and spin fluctuations. This coexistence is a distinctive feature of the AFM2 phase as a whole and not a superposition of dynamical responses from the AFM1 phase and the PM state.

Previous neutron diffraction measurements performed under a magnetic field in powder and single crystal samples indicate a transition from the AFM1 to the AFM2 phase at 3.5 T for 58 K [15,18]. The full magnetic phase diagram as a function of temperature and magnetic field up to 10 T applied along the c axis was established by electrical transport and magnetization measurements [20] and is sketched in Fig. 4(a). Below 60 K, the increasing magnetic field induces transitions from the AFM1 to another intermediate AFM1′ phase before reaching the AFM2 phase. Above 60 K, the AFM2 phase is stable up to the maximum investigated field of 10 T.

Building upon these results, we investigated the field dependence of the magnetic Bragg peak intensities (1, 2, 0)

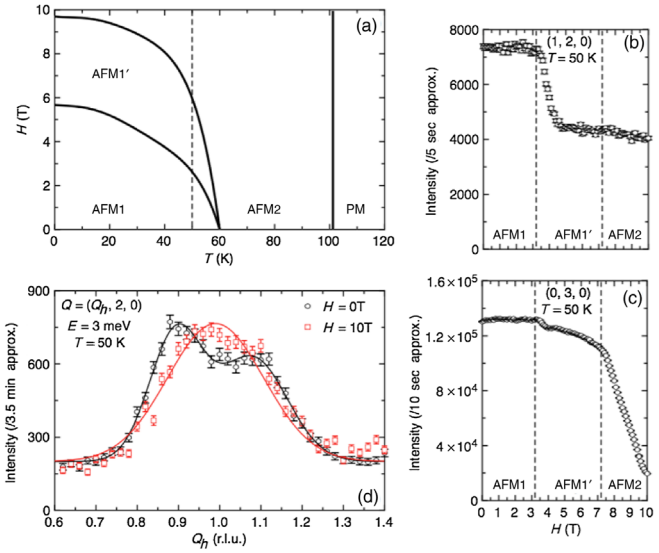

FIG. 4. (a) (T-H) phase diagram of Mn_5Si_3 for $\vec{H}\|c$ after Ref. [20]. The vertical dashed line indicates the temperature (50 K) where neutron scattering measurements were performed under a magnetic field. (b),(c) Field dependence of magnetic Bragg peaks (1, 2, 0) and (0, 3, 0) at 50 K. For (1, 2, 0), a 9 mm plexiglass attenuator was in place. (d) Inelastic spectra obtained at 50 K around $\mathbf{Q} = (Q_h, 2, 0)$ under a 0 and 10 T magnetic field for an energy transfer of 3 meV. The red line is a guide for the eyes, and the black line corresponds to fits with Gaussian functions. Data were obtained with an unpolarized neutron beam using IN12.

and (0, 3, 0) for a field applied along the c axis at $T = 50$ K [see Figs. 4(b) and 4(c)]. This temperature was chosen well within the AFM1 phase (at $H = 0$ T), where critical fluctuations from the AFM2 to the AFM1 transition are absent. Starting at $H = 0$ T in the AFM1 phase, two anomalies at approximatively 3 and 7 T mark the onset of different magnetic phases that are identified as the AFM1′ and AFM2 phases, roughly consistent with the (T-H) phase diagram of Ref. [20]. The intermediate AFM1′ phase is not addressed in this Letter. Above 7 T, the system reenters the AFM2 phase characterized by a drop of a factor ≈ 2 compared to AFM1 in the intensity of the Bragg peak (1, 2, 0) and a continuous diminution of the (0, 3, 0) Bragg peak intensity. Up to the maximum investigated field of 10 T, the PM state is not reached, which is related to the very steep $T_{N_2}(H)$ phase boundary. The field induced AFM2 phase at 50 K consists of AFM coupled magnetic moments lying perpendicular to H with an additional increasing induced FM component, which is evidenced in magnetization measurements [20].

Figure 4(d) shows INS spectra collected around $\mathbf{Q} = (Q_h, 2, 0)$ at 50 K at a constant energy transfer of $E = 3$ meV for $H = 0$ and 10 T. The typical spin-wave spectra with two peaks in the AFM1 phase at $H = 0$ T transforms into a broad peak centered at the magnetic center $Q_h = 1$ r.l.u. at 10 T. The modification of the magnetic excitation spectrum at 50 K as a function of magnetic field [Fig. 4(d)] is identical to the one as a function of temperature at $H = 0$ T [Fig. 2(d)], and therefore one concludes that the field restores the fluctuation pattern associated with the AFM2 phase. This leads to the unusual behavior in which a high enough magnetic field of 10 T applied in the AFM1 phase induces spin fluctuations. Indeed, this feature is surprising due to a sizable induced FM component of about $0.6\mu_B$ for a field of 10 T at $T = 50$ K [18,20]. By contrast, a field of 10 T applied in the AFM2 phase and PM state reduces the intensity of the magnetic excitations without changing their line shapes (see the Supplemental Material [23]).

The microscopic ingredients giving rise to the stability of the mixed magnetism of the AFM1 and AFM2 phases, constituted of the coexistence of magnetic and nonmagnetic sites, were discussed in previous studies on Mn_5Si_3 [15–18,20]. Namely, a first ingredient at play is the Mn1-Mn1 distance with respect to the critical value corresponding to the instability in the competition between bonding and magnetism. The shortest Mn1-Mn1 distance in Mn_5Si_3 equals $c/2$ and is too small in the AFM2 state to lead to a magnetic configuration for Mn1. Below T_{N1}, an abrupt change of the lattice parameter value c occurs, and this stabilizes the magnetic configuration of the Mn1 site. Under a magnetic field, it was shown with a neutron diffraction experiment performed at 50 K and 4 T [15] that $c/2$ decreases below the critical value for Mn1 moment stability. A second ingredient common to the AFM1 and AFM2 phases is the geometrical frustration associated with the triangular arrangement of Mn2 atoms, which leads to the occurrence of two ordered moments out of the three Mn2 sites [see Fig. 1(a)].

The evidenced spin fluctuations within a magnetically ordered phase are related to the presence of nonmagnetic Mn sites in Mn_5Si_3. Such a mixed magnetic phase is shared among several Mn-based systems, e.g., elemental Mn [28,29] and the Laves phases RMn_2 (with R being a rare earth element) [30]. In particular, these phases are studied for fundamental magnetic properties [30], as well as for the MCE [31]. In RMn_2 systems, the same ingredients as in Mn_5Si_3 are at play: instability of Mn magnetism and magnetic frustration. The switch from a conventional to a mixed AFM phase as a function of magnetic field was theoretically predicted and verified by neutron diffraction experiments in $TbMn_2$ [32]. This situation bears similarity to Mn_5Si_3, and our results are echoed in the broader context of mixed magnetic system studies. This Letter goes one step further by evidencing the properties of the excitation spectrum of the mixed magnetic phases, revealing the coexistence of two dynamical responses, spin waves and spin fluctuations.

Another important result of our Letter is the evidence of magnetic field induced spin fluctuations. Starting from the AFM1 phase, which sustains only spin waves, the field restores the AFM2 phase and its associated spin fluctuations. In contrast to the discrete spin-wave spectrum, such

spin fluctuations which consist of a continuum of excitations involve more microscopic states. This leads to an increase in the magnetic entropy and thus plays a major role in the inverse MCE. It is to be noted that the observed behavior is the opposite of the most common magnetic field effect that usually suppresses the spin fluctuations and, consequently, decreases the magnetic entropy. The latter leads to the direct MCE, as recently demonstrated by INS in the FM MCE compound $MnFe_4Si_3$ [33].

In summary, we evidence the coexistence of spin waves and spin fluctuations in the high temperature mixed AFM phase of Mn_5Si_3. We show that the modification of the magnetic excitation spectrum induced by the magnetic field tracks the inverse MCE via the associated change of magnetic entropy. This effect is likely to be valid beyond the specific sequence of magnetic transitions of Mn_5Si_3. Therefore, our Letter strongly suggests reinvestigating systems where Mn is on the verge of a magnetic stability in view of magnetocaloric applications. The need to design functional materials for magnetic refrigeration connects with a fundamental understanding of magnetism.

*n.biniskos@fz-juelich.de
†raymond@ill.fr

[1] A. M. Tishin and Y. I. Spichkin, *The Magnetocaloric Effect and Its Applications* (IOP Publishing, Bristol, England, 2003).
[2] W. F. Giauque and I. P. D. McDougall, Attainment of temperatures below 1° absolute by demagnetization of $Gd_2(SO_4)_3 \cdot 8H_2O$, Phys. Rev. **43**, 768 (1933).
[3] V. K. Pecharsky and K. A. Gschneidner, Jr., Giant Magnetocaloric Effect in $Gd_5(Si_2Ge_2)$, Phys. Rev. Lett. **78**, 4494 (1997).
[4] O. Tegus, E. Brück, K. H. J. Buschow, and F. R. de Boer, Transition-metal-based magnetic refrigerants for room-temperature applications, Nature (London) **415**, 150 (2002).
[5] J. Lyubina, K. Nenkov, L. Schultz, and O. Gutfleisch, Multiple Metamagnetic Transitions in the Magnetic Refrigerant $La(Fe, Si)_{13}H_x$, Phys. Rev. Lett. **101**, 177203 (2008).
[6] B. Yu, M. Liu, P. W. Egolf, and A. Kitanovski, A review of magnetic refrigerator and heat pump prototypes built before the year 2010, Int. J. Refrig. **33**, 1029 (2010).
[7] T. Krenke, E. Duman, M. Acet, E. F. Wassermann, X. Moya, L. Mañosa, and E. Planes, Inverse magnetocaloric effect in ferromagnetic Ni-Mn-Sn alloys, Nat. Mater. **4**, 450 (2005).
[8] J. Liu, T. Gottschall, K. P. Skokov, J. D. Moore, and O. Gutfleisch, Giant magnetocaloric effect driven by structural transitions, Nat. Mater. **11**, 620 (2012).
[9] O. Tegus, E. Brück, L. Zhang, Dagula, K. H. J. Buschow, and F. R. de Boer, Magnetic phase transitions and magnetocaloric effects, Physica (Amsterdam) **319B**, 174 (2002).
[10] Y. Q. Zhang and Z. D. Zhang, Giant magnetoresistance and magnetocaloric effects of the $Mn_{1.82}V_{0.18}Sb$ compound, J. Alloys Compd. **365**, 35 (2004).
[11] S. A. Nikitin, G. Myalikgulyev, A. M. Tishin, M. P. Annaorazov, K. A. Asatryan, and A. L. Tyurin, The magnetocaloric effect in $Fe_{49}Ni_{51}$ compound, Phys. Lett. A **148**, 363 (1990).
[12] T. Tohei, H. Wada, and T. Kanomata, Negative magnetocaloric effect at the antiferromagnetic to ferromagnetic transition of Mn_3GaC, J. Appl. Phys. **94**, 1800 (2003).
[13] W. J. Hu, J. Du, B. Li, Q. Zhang, and Z. D. Zhang, Giant magnetocaloric effect in the Ising antiferromagnet DySb, Appl. Phys. Lett. **92**, 192505 (2008).
[14] D. Songlin, O. Tegus, E. Brück, J. C. P. Klaasse, F. R. de Boer, and K. H. J. Buschow, Magnetic phase transition and magnetocaloric effect in $Mn_{5-x}Fe_xSi_3$, J. Alloys Compd. **334**, 249 (2002).
[15] M. Gottschilch, O. Gourdon, J. Persson, C. de la Cruz, V. Petricek, and T. Brückel, Study of the antiferromagnetism of Mn_5Si_3: An inverse magnetocaloric effect material, J. Mater. Chem. **22**, 15275 (2012).
[16] P. J. Brown and J. B. Forsyth, Antiferromagnetism in Mn_5Si_3: The magnetic structure of the AF2 phase at 70 K, J. Phys. Condens. Matter **7**, 7619 (1995).
[17] P. J. Brown, J. B. Forsyth, V. Nunez, and F. Tasset, The low-temperature antiferromagnetic structure of Mn_5Si_3 revised in the light of neutron polarimetry, J. Phys. Condens. Matter **4**, 10025 (1992).
[18] M. R. Silva, P. J. Brown, and J. B. Forsyth, Magnetic moments and magnetic site susceptibilities in Mn_5Si_3, J. Phys. Condens. Matter **14**, 8707 (2002).
[19] L. Vinokurova, V. Ivanov, E. Kulatov, and A. Vlasov, Magnetic phase transitions and electronic structure of the manganese silicides, J. Magn. Magn. Mater. **90–91**, 121 (1990).
[20] C. Sürgers, T. Wolf, W. Adelmann, W. Kittler, G. Fischer, and H. v. Löhneysen, Switching of a large anomalous Hall effect between metamagnetic phases of a non-collinear antiferromagnet, Sci. Rep. **7**, 42982 (2017).
[21] C. Sürgers, G. Fischer, P. Winkel, and H. v. Löhneysen, Large topological Hall effect in the non-collinear phase of an antiferromagnet, Nat. Commun. **5**, 3400 (2014).
[22] C. Sürgers, W. Kittler, T. Wolf, and H. v. Löhneysen, Anomalous Hall effect in the noncollinear antiferromagnet Mn_5Si_3, AIP Adv. **6**, 055604 (2016).
[23] See Supplemental Material at http://link.aps.org/supplemental/10.1103/PhysRevLett.120.257205, which includes Refs. [24–27], for supporting information and experimental details.
[24] M. Kempa, B. Janousova, J. Saroun, P. Flores, M. Boehm, F. Demmel, and J. Kulda, The FlatCone multianalyzer setup for ILL's three-axis spectrometers, Physica (Amsterdam) **385–386B**, 1080 (2006).
[25] L. P. Regnault, B. Geffray, P. Fouilloux, B. Longuet, F. Mantegazza, F. Tasset, E. Leliévre-Berna, S. Pujol, E. Bourgeat-Lami, N. Kernavanois, M. Thomas, and Y. Gibert, Spherical neutron polarization analysis on the three-axis spectrometer IN22, Physica (Amsterdam) **350B**, E811 (2004).
[26] K. Schmalzl, W. Schmidt, S. Raymond, H. Feilbach, C. Mounier, B. Vettard, and T. Brückel, The upgrade of the cold neutron three-axis spectrometer IN12 at the ILL, Nucl. Instrum. Methods Phys. Res., Sect. A **819**, 89 (2016).

[27] T. Chatterji, *Neutron Scattering from Magnetic Materials* (Elsevier, Amsterdam, 2006).

[28] T. Yamada, N. Kunitomi, Y. Nakai, D. E. Cox, and G. Shirane, Magnetic structure of α-Mn, J. Phys. Soc. Jpn. **28**, 615 (1970).

[29] D. Hobbs, J. Hafner, and D. Spišák, Understanding the complex metallic element Mn. I. Crystalline and noncollinear magnetic structure of α-Mn, Phys. Rev. B **68**, 014407 (2003).

[30] R. Ballou, Geometric frustration in rare earth antiferromagnetic compounds, J. Alloys Compd. **275–277**, 510 (1998).

[31] W. Zuo, F. Hu, J. Sun, and B. Shen, Large reversible magnetocaloric effect in RMn_2 ($R =$ Tb, Dy, Ho, Er) compounds, J. Alloys Compd. **575**, 162 (2013).

[32] R. Ballou, B. Ouladdiaf, P. J. Brown, M. D. N. Regueiro, and C. Lacroix, Unusual field-induced transition in a frustrated itinerant antiferromagnet, Phys. Rev. B **45**, 3158 (1992).

[33] N. Biniskos, S. Raymond, K. Schmalzl, A. Schneidewind, J. Voigt, R. Georgii, P. Hering, J. Persson, K. Friese, and T. Brückel, Spin dynamics of the magnetocaloric compound $MnFe_4Si_3$, Phys. Rev. B **96**, 104407 (2017).